Size effects on brittle fracture of Brazilian disk samples containing a circular hole

# Size effects on brittle fracture of Brazilian disk samples containing a circular hole

A.R. Torabi[a], S. Etesam[a], A. Sapora [b]*, P. Cornetti[b]

[a] *Fracture Research Laboratory, Faculty of New Sciences & Technologies, University of Tehran, P.O. Box 14395-1561, Tehran, Iran*

[b] *Department of Structural, Geotechnical and Building Engineering, Politecnico di Torino, 10129, Torino, Italy*

* Corresponding Author: alberto.sapora@polito.it

## Abstract

Brittle fracture tests are carried out on Brazilian disk (BD) specimen containing a circular hole. The experimental campaign involves two different brittle materials, Polymethyl-methacrylate (PMMA) and general-purpose Polystyrene (GPPS), respectively. Keeping fixed the disk diameter, five different hole sizes are tested for each material sample, thus allowing a full description of the size effects related to the geometry under investigation. The recorded failure stresses are compared with theoretical predictions by the coupled Finite Fracture Mechanics (FFM) criterion, which is implemented by means of analytical relationships for the stress field and the stress intensity factor (SIF) available in the Literature. The agreement is generally satisfactory, except from very small holes, where some nonlinear effects influenced the failure mechanisms.

***Keywords*:** BD tests, circular hole, size effects, FFM

## 1. Introduction

Linear elastic notch fracture mechanics (LENFM) was born about twenty years ago as a new branch of the fracture mechanics in which the fracture behaviour of notched engineering components and structures made of linear elastic materials is investigated. By means of the failure criteria in the context of LENFM, it is possible to predict fracture of brittle and quasi-brittle notched structures and prevent catastrophic failures.

From the viewpoint of geometry, notches appear in various shapes among which V-, U- and O-shaped (i.e. circular) notches are the most usual ones. Depending on the notch geometry, e.g. the notch angle, the notch tip radius etc., the level of stress concentration and particularly that of stress

gradient at the notch vicinity is different. As a result, some brittle fracture criteria may be accurate for some specific notch geometries and inaccurate for some others. Therefore, it is essential to evaluate the effectiveness of various brittle fracture criteria for different notch shapes and determine appropriate criteria for each notch shape. Dealing with brittle fracture of notched domains, several failure criteria have been already proposed in the literature and verified by means of extensive experimental results obtained from different materials, specimens and notch shapes. The most active criteria are namely the maximum hoop stress and mean stress criteria [1-4], whose concept have been taken from the well-known Theory of Critical Distances [5,6], the Averages Strain Energy Density criterion [7-10], the Cohesive Zone Model (CZM) [11-13], and FFM [14,15].

A general survey of industrial components and structures indicates that circular notch (i.e. O-shaped notch) is really the most applied notch shape utilized for various purposes such as connecting two or more parts together by means of bolts, screws, rivets etc. In case circular notches are introduced in structures made of brittle or quasi-brittle materials, sudden or at least rapid fracture may take place, leading to heavy damage of the structures. Although for a large number of O-notched structures brittle fracture can be accurately predicted by means of the classic strength of materials, i.e. by using the stress concentration factor, there are several cases for which the level of stress concentration is so high that using the implementation of LENFM criteria for brittle fracture prediction is inevitable.

In the present research, brittle fracture is investigated experimentally and theoretically in circular notches under pure opening mode. Fracture experiments are carried out on the Brazilian disk (BD) specimen weakened by a central circular hole and made of PMMA or GPPS. With the aim to study the effects of notch size on the fracture behaviour of the specimens, BD samples are fabricated and tested with different hole radii. Experimental results are interpreted in terms of FFM. The coupled FFM criterion in its average form, i.e. by coupling an average stress condition with the energy balance [14], can be expressed as (see Fig. 1a for the frame of reference, $R$ being the hole radius):

$$\begin{cases} \dfrac{1}{\Delta}\displaystyle\int_{R}^{R+\Delta} \sigma_x(y)dy = \sigma_u \\ \dfrac{1}{\Delta}\displaystyle\int_{0}^{\Delta} K_I^2(a)da = K_{Ic}^2 \end{cases} \tag{1}$$

where $\sigma_x$ is the tensile stress along the axial loading, $\sigma_u$ is the tensile strength, $K_I$ is the SIF related to a crack of length $a$ stemming from the notch tip, and $K_{Ic}$ is the fracture toughness. According to FFM, fracture takes place through a finite discrete crack advance $\Delta$. Its critical value $\Delta_c$ represents one the two unknowns of system (1) at incipient failure, together with the nominal failure stress $\sigma_f$,

which is embedded in the functions $\sigma_x$ and $K_I$ as it will be shown in Section 2. Note that the crack advance is not a mere material function as for other criteria based on a finite distance [3,4,16]. According to FFM, $\Delta_c$ becomes a structural parameter, depending also on the geometry [14,15], and the loading conditions [17-19].

Finally, let us remark that FFM has been already applied to investigate failure initiation from a circular hole in brittle elements, providing good results for composite materials [20,21], and generally mediocre predictions for polymeric materials [22-24]. In this spirit, the present manuscript represents the complementary work of that presented in [25], where tensile tests were carried out both on PMMA and GPPS notched elements, and the related experimental data were successfully interpreted by means of FFM.

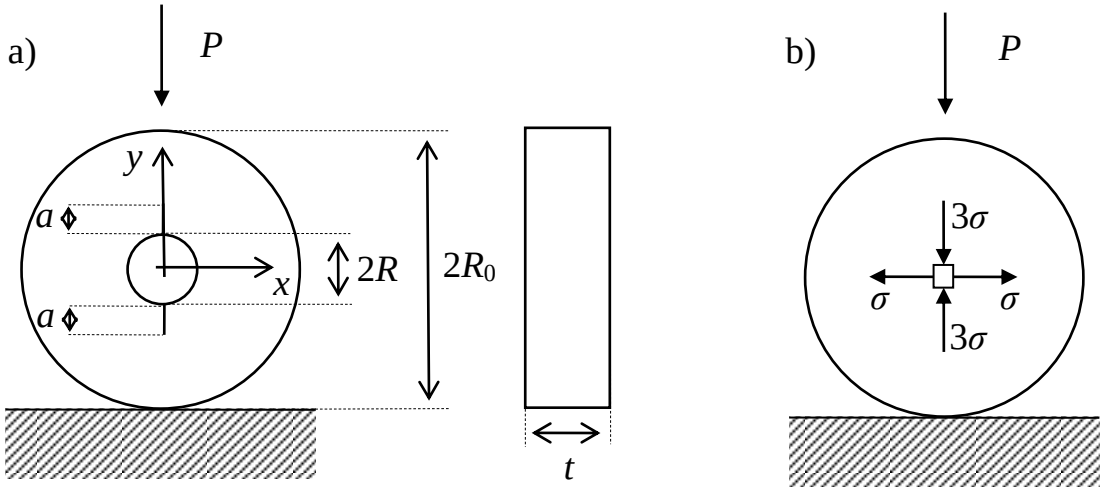


**Figure 1.** BD tests: a) notched sample geometry: the presence of symmetric cracks of length *a* stemming from the notch tips is also represented; b) stress distribution at the centre of the disk for a plain specimen.

## 2. Stress field and SIF function

For the BD samples depicted in Fig. 1a, the stress field $\sigma_x(y)$ can be expressed analytically for a vanishing radius *R*. Let us observe that for a plain specimen the normal stress is positive, approximately constant (except from the extreme/contact zones) and equal to $\sigma$ along the loading axis *y*, whit [26,27]

$$\sigma = \frac{P}{\pi R_0 t} \tag{2}$$

On the contrary, the normal stress is negative along the orthogonal axis *x*, reaching its minimum $-3\sigma$ at the centre of diameter (Fig. 1b). Kirsch solution thus yields:

$$\sigma_x(y) = \frac{\sigma}{2}\left(2 - 2\frac{R^2}{y^2} + 12\frac{R^4}{y^4}\right) \tag{3}$$

Equation (3) provides ideally a stress concentration factor $\sigma_x(y=R)/\sigma = 6$, meaning that the maximum stress is 6 times higher than the nominal one, i.e. the stress in absence of a hole. Note that the stress concentration factor is equal twice that related to a tensile plate containing a circular hole [25]. Indeed, the accuracy of the stress field (3) for not negligible $R/R_0$ ratios could be improved by taking the following multiplying factor into account [26,27]:

$$F_{corr} = 1 + \frac{19}{3}\left(\frac{R}{R_0}\right)^2 \tag{4}$$

The precision of Eq. (4) has been checked by a finite element analysis for the geometries under investigation (Section 3), providing significant results starting from $R/R_0=0.1$.

On the other hand, for sufficiently small hole radii, the SIF function related to a crack of length *a* stemming from the notch can be approximated with the one valid for a circular hole in an infinite plate, where [28]

$$K_I(a) = \sigma\sqrt{\pi a}\,F(s) \tag{5}$$

with

$$s = \frac{a}{a+R} \tag{6}$$

The shape function *F* related to the symmetric crack propagation (Fig. 1a), which in this case has to preferred with respect to an asymmetric one [25] (for a deeper insight on symmetric vs. asymmetric crack initiation, see [29,30]), can be written as:

$$F(s) = (1-\lambda)F_0(s) + \lambda F_1(s) \tag{7}$$

where

$$F_0(s) = 0.5\,(3-s)\,[1+1.243(1-s)^3] \tag{8a}$$

$$F_1(s) = 1+\,(1-s)\,[0.5+0.743(1-s)^2] \tag{8b}$$

and $\lambda = -3$ according to the present geometry (Fig. 1b).

## 3. Experimental investigation

BD tests were carried out in the Fracture Research Laboratory of the University of Tehran on notched disks made of two different brittle materials, PMMA and GPPS, respectively. By referring to the sample geometry depicted in Fig. 1a, the diameter $2R_0$ was fixed equal to 80 mm, and the thickness was chosen large enough to achieve plane strain conditions: $t$ = 10 mm for PMMA samples, and $t$ = 8 mm for GPPS samples. Five different hole sizes were considered with the following dimensions: $2R$ = 0.5, 1, 2, 4, and 8 mm. Three different samples were fabricated and tested for each hole size, for a total of 30 BD tests carried out (Fig. 2). The test speed was set equal to 0.5 mm/min in order to prevent possible instabilities in the compression tests. To fabricate BD samples, first, rectangular plates of PMMA and GPPS were provided. Then, the outer boundary of BD was cut by means of the water-jet cutting machine. An accurate machining process enabled us to get precise hole size . Finally, to remove possible stress raisers at the boundaries remained from the cutting processes, they were polished by means of fine abrasive papers.

The experimental fracture was of brittle character, but increasing non-linearities were observed in the force-displacement curves for decreasing hole sizes, becoming evident for $R$=0.25 mm as shown in Fig. 3.

Recorded failure loads $P_f$ for all the tests are reported in Table 1. From these values, the nominal stress at failure $\sigma_f$ can be evaluated from Eq. (2). On the other hand, from the failure load related to the largest hole size ($R$=4 mm, Table 1), the following relationship provide a good estimate for the tensile strength $\sigma_u$ [29]:

$$\sigma_u = \frac{P_f}{\pi R_0 t}\left(6 + 38\left(\frac{R}{R_0}\right)^2\right) \tag{9}$$

The application of Eq. (9) for $R$=4 mm and $R_0$=40 mm yields $\sigma_u$ = 78 MPa for PMMA, and $\sigma_u$ = 40 MPa for GPPS. In the following section, typical values for the fracture toughness will be implemented: $K_{Ic}$ = 1.75 MPa $\sqrt{\text{m}}$ for PMMA (thus, $l_{ch} = (K_{Ic}/\sigma_u)^2 \simeq 0.503\,\text{mm}$), and $K_{Ic}$ = 0.9 MPa $\sqrt{\text{m}}$ for GPPS (thus, $l_{ch} = (K_{Ic}/\sigma_u)^2 \simeq 0.506\,\text{mm}$). Interestingly, the values of $l_{ch}$ for the two materials are very close with each other: since the sample geometry was identical (except from the thickness $t$), and since $l_{ch}$ estimates the order of magnitude of the crack advance $\Delta_c$ [14,15], a similar trend for FFM predictions on the two data sets is expected.

Eventually, note that the material properties for PMMA and GPPS differ from those implemented in [25], since the material plate from which samples were machined was not the same.

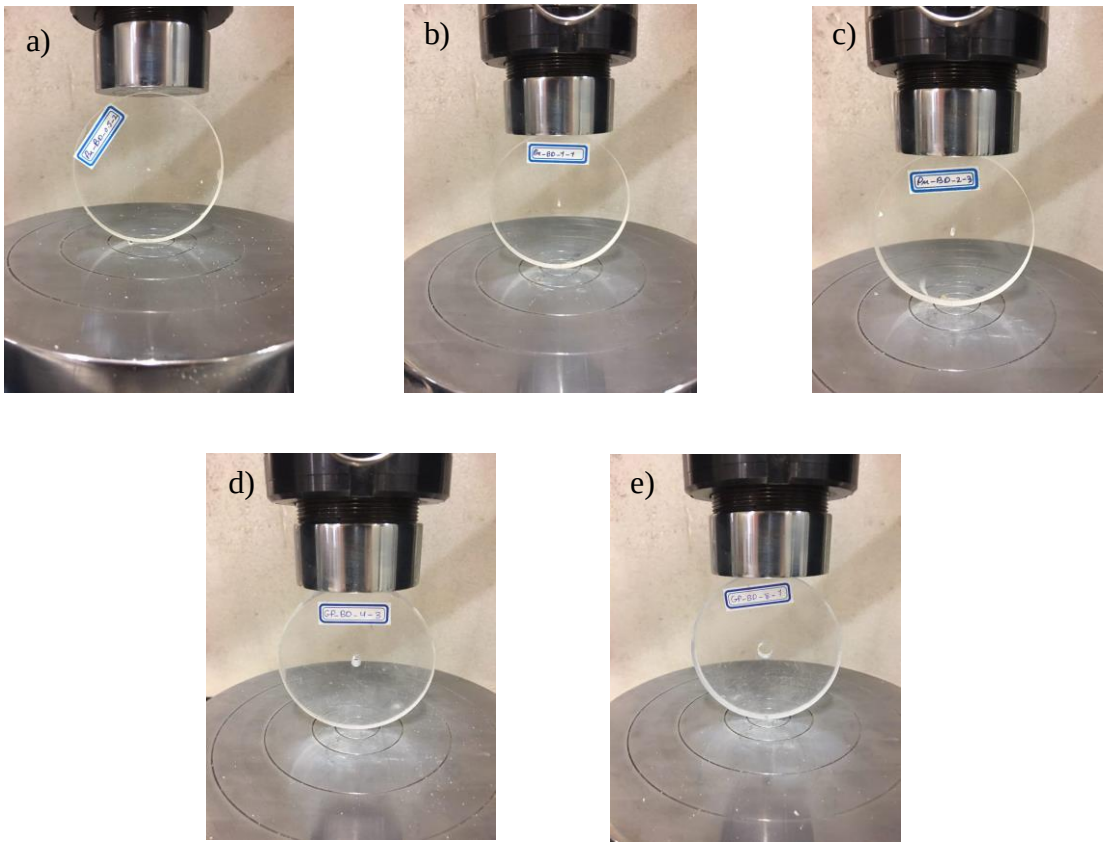


**Figure 2.** BD tested samples: a) 2*R*=0.5 mm (PMMA); b) 2*R*= 1 mm (PMMA); c) 2*R*=2 mm (PMMA); d) 2*R*=4 mm (GPPS); e) 2*R*= 8 mm (GPPS).

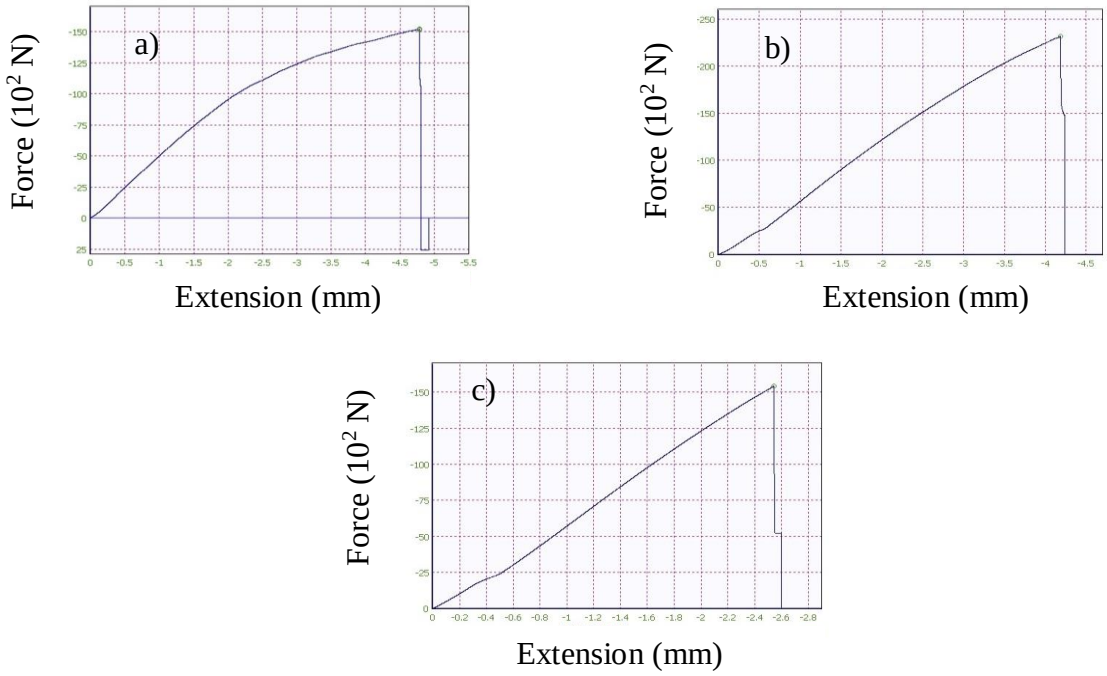


**Figure 3.** Force-extension curves recorded during experiments: a) 2*R*=0.5 mm (GPPS); b) 2*R*= 2 mm (PMMA); c) 2*R*= 8 mm (PMMA).

| PMMA | | | GPPS | | |
|---|---|---|---|---|---|
| Hole diameter 2*R* (mm) | Failure load $P_f$ (N) | Average failure load (N) | Hole diameter 2*R* (mm) | Failure load $P_f$ (N) | Average failure load (N) |
| 0.5 | 37150 | 35660 | 0.5 | 15930 | 15100 |
| 0.5 | 33810 | | 0.5 | 15280 | |
| 0.5 | 36020 | | 0.5 | 14090 | |
| 1 | 28800 | 27650 | 1 | 12260 | 12050 |
| 1 | 26230 | | 1 | 11970 | |
| 1 | 27920 | | 1 | 11920 | |
| 2 | 21830 | 23210 | 2 | 9950 | 9360 |
| 2 | 24700 | | 2 | 9130 | |
| 2 | 23100 | | 2 | 9000 | |
| 4 | 20250 | 19420 | 4 | 8070 | 7760 |
| 4 | 19936 | | 4 | 7645 | |
| 4 | 18074 | | 4 | 7565 | |
| 8 | 14414 | 15338 | 8 | 6525 | 6310 |
| 8 | 16168 | | 8 | 6220 | |
| 8 | 15432 | | 8 | 6185 | |

**Table 1.** BD tests: failure loads recorded during experiments on both PMMA and GPPS notched samples.

## 4. FFM predictions

The FFM criterion (1) can be now implemented by means of Eqs. (3) and (5). By introducing the function *f* related to the integration of the stress field (3) and the function *g* related to the integration of the SIF squared (3), some analytical manipulations allow to write the FFM system at failure as:

$$\begin{cases} f\left(\Delta_c / R\right) - \sqrt{l_{ch}\, g\left(\Delta_c / R\right)} = 0 \\ \dfrac{\sigma_f}{\sigma_u} = \dfrac{\Delta_c / R}{f\left(\Delta_c / R\right)} \end{cases} \tag{10}$$

Once the radius $R$ and the material properties are fixed, from the former equation in (10) it is possible to get the critical crack advance $\Delta_c$, which must be then substituted into the latter equation to estimate the failure stress $\sigma_f$.

Results related to both PMMA and GPPS are reported in Fig. 4, whereas the percentage discrepancy from the average experimental data is shown in Fig. 5. The size effects are well-caught by FFM, and the trend of theoretical predictions is similar for both materials. As can be seen, FFM results are good for $R$=4, 2, 1, and 0.5 mm, with discrepancies below 13%. On the other hand, the accuracy decreases (discrepancies above 20%) for the smallest hole, i.e., $R$=0.25 mm.

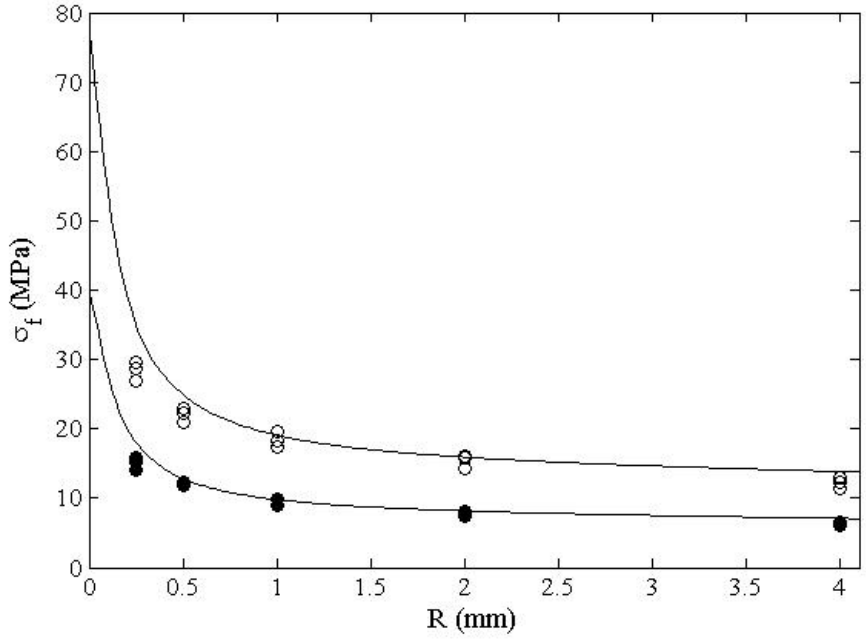


**Figure 4**. BD notched samples: failure stress according to FFM (continuous line), and to experimental tests on PMMA (plain circles) and GPPS (black circles).

Looking for a possible explanation, it should be noted once again that the force-displacement curves (Figure 3) become nonlinear as the radius $R$ decreases, and this trend is evident for $R$=0.25 mm. The nonlinear behaviour is related to the high fracture load necessary for failure, activating some alternative damage mechanisms in BD specimens, since tested under remote compression. Note that shearing stresses could be also induced in plain samples (and thus in sample containing very small holes) and sometimes failure starts from loading points with the generation of wedges [26,27]. As a matter of fact, this nonlinear behaviour was not observed in [25], where tensile tested samples contained circular holes with the same radius $R$ and the same radius to width ratio.

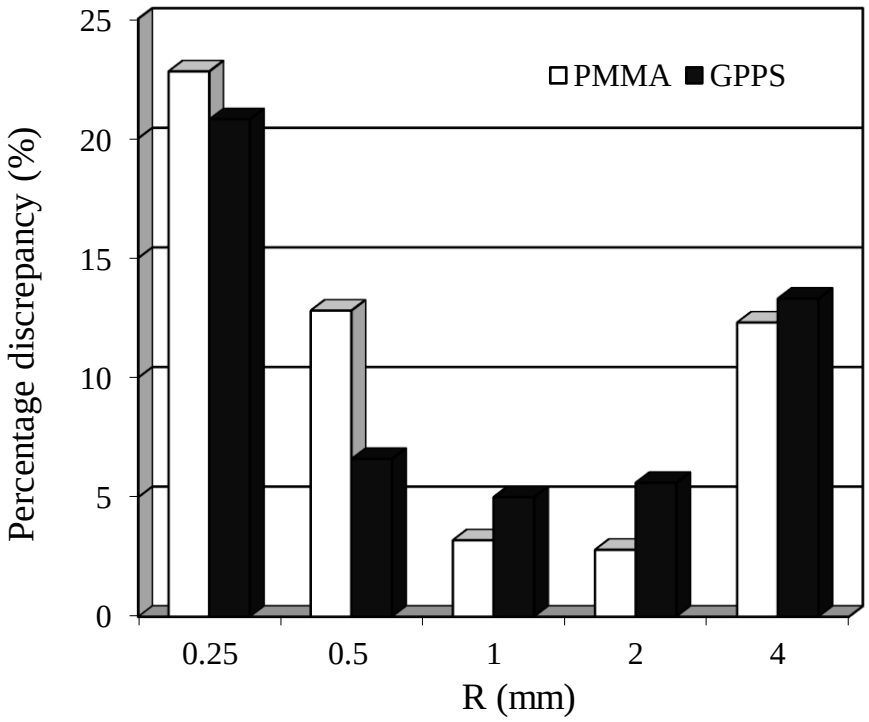


**Figure 5.** Percentage discrepancy between FFM predictions and mean experimental values related to BD tests on PMMA and GPPS notched samples.

Finally, Fig. 6 shows the critical crack advance $\Delta_c$ for PMMA samples, which depends on the radius $R$ and on the material properties. If the correction factor $F_{corr}$ (Eq. (4)) is disregarded, the values of $\Delta_c$ lie between $2/\pi\ l_{ch}$ for $R/l_{ch} << 1$, and $2/\pi\ (1.12)^2\ l_{ch}$ for and $R/l_{ch} >> 1$. On the other hand, by considering $F_{corr}$ as it was done in our analysis, $\Delta_c$ starts increasing as larger radii are taken into account. Nearly coincident values are obtained for GPPS samples.

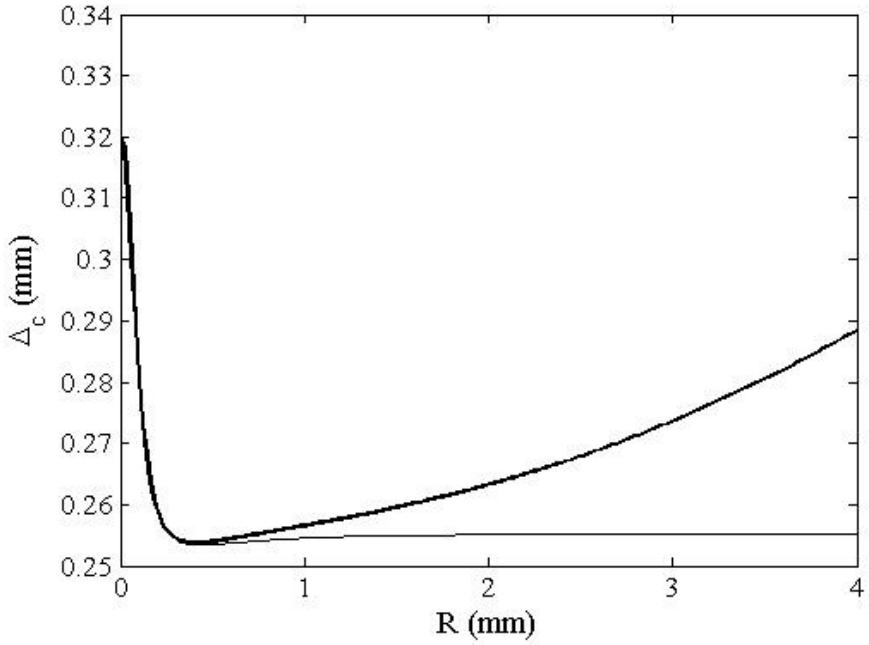


**Figure 6**. BD notched samples made of PMMA: FFM critical crack advance obtained by neglecting (thin line) or by considering (thick line) the correction factor (4) for the stress field (3).

## 5. Conclusions

Size effects related to circular notched samples describe that the strength $\sigma_f$ of the structure decreases as the hole radius $R$ increases. Particularly, referring to the case of a BD infinite geometry ($R<<R_0$), $\sigma_f$ varies ideally between $\sigma_u$ (plain/integer sample, $R$=0) and $\sigma_u/6$ ($R>>l_{ch}$). For finite geometries, some correction factor should be taken into account. In the present manuscript this trend is caught both experimentally, by testing PMMA and GPPS notched samples, and theoretically by means of the coupled FFM criterion. Actually, FFM predictions are accurate but for small hole sizes, where the failure stress is overestimated of more than 20%: this discrepancy is imputable to some nonlinear phenomena (detected in the stress-displacement curves) related to the high failure load and the particular (compressive) loading conditions. The investigation of nonlinearities goes beyond the scope of the paper, but some works are in progress following the analysis presented in [31], where nonlinear effects observed during failure were modelled trough the FFM criterion in the regime of small scale yielding.

## References

[1] Ayatollahi, M.R., Torabi, A.R. Brittle fracture in rounded-tip V-shaped notches. Materials & Design 2010; 31: 60-67.

[2] Ayatollahi, M.R., Torabi, A.R. Tensile fracture in notched polycrystalline graphite specimens. Carbon 2010; 48: 2255-2265.

[3] Torabi, A.R., Fakoor, M., Pirhadi, E. Tensile fracture in coarse-grained polycrystalline graphite weakened by a U-shaped notch. Engineering Fracture Mechanics 2013; 111:77-85.

[4] Torabi, A.R. Sudden Fracture from U-Notches in Fine-Grained Isostatic Graphite Under Mixed Mode I/II Loading. International Journal of Fracture 2013; 181: 309-316.

[5] Taylor, D. Predicting the fracture strength of ceramic materials using the theory of critical distances. Engineering Fracture Mechanics 2004;71:2407–2416.

[6] Kasiri, S., Taylor, D. A critical distance study of stress concentrations in bone. J Biomech 2008; 41:603–609.

[7] Lazzarin, P., Zambardi, R. A finite-volume-energy based approach to predict the static and fatigue behavior of components with sharp V-shaped notches. International Journal of Fracture 2001; 112: 275-298.

[8] Berto, F., Lazzarin, P., Ayatollahi, M.R. Brittle fracture of sharp and blunt V-notches in isostatic graphite under torsion loading. Carbon 2012; 50: 1942-1952.

[9] Berto, F., Ayatollahi, M.R. Fracture assessment of Brazilian disc specimens weakened by blunt V-notches under mixed mode loading by means of local energy. Materials & Design 2011; 32: 2858-2869.

[10] Berto, F., Cendon, D.A., Lazzarin, P. et al. Fracture behaviour of notched round bars made of PMMA subjected to torsion at −60°C. Engineering Fracture Mechanics 2013; 102: 271-287.

[11] Gomez, F., Guinea, G., Elices, M. Failure criteria for linear elastic materials with U-notches. International Journal of Fracture 2006; 141: 99-113.

[12] Gómez, F.J., Elices, M. A fracture criterion for sharp V-notched samples. International Journal of Fracture 2003; 123: 163-175.

[13] Cendón, D.A., Torabi, A.R., Elices, M. Fracture assessment of graphite V-notched and U-notched specimens by using the cohesive crack model. Fatigue & Fracture of Engineering Materials & Structures 2015; 38: 563-573.

[14] Carpinteri, A., Cornetti, P., Pugno, N., Sapora, A., Taylor, D. Generalized fracture toughness for specimens with re-entrant corners: experiments vs. theoretical predictions, Struct. Eng. Mech. 2009; 32: 609–620.

[15] Sapora, A., Cornetti, P., Carpinteri, A., Firrao, D. An improved Finite Fracture Mechanics approach to blunt V-notch brittle fracture mechanics: Experimental verification on ceramic, metallic, and plastic materials, Theoretical and Applied Fracture Mechanics 2015; 78, 20–24.

[16] Berto, F., Lazzarin, P. Recent developments in brittle and quasi-brittle failure assessment of engineering materials by means of local approaches, Materials Science and Engineering R 2014; 75, 1–48.

[17] Cornetti, P., Sapora, A., Carpinteri, A. T-stress effects on crack kinking in finite fracture mechanics, Engineering Fracture Mechanics 2014; 132:169–176.

[18] Sapora, A., Cornetti, P., Carpinteri V-notched elements under mode II loading conditions, Structural Engineering and Mechanics 2014; 49:499-508.

[19] Campagnolo, A., Berto, F. , Leguillon, D. Fracture assessment of sharp V-notched components under Mode II loading: a comparison among some recent criteria. Theoretical and Applied Fracture Mechanics 2016; 85: 217–226.

[20] Camanho, P.P., Erçin, G., Catalanotti, G., Mahdi, D., Linde, P. A finite fracture mechanics model for the prediction of the open-hole strength of composite laminates, Composites Part A: Applied Science and Manufacturing 2012; 43:1219–1225.

[21] Furtado C., Arteiro A., Bessa M.A., Wardle B.L., Camanho P.P. Prediction of size effects in open-hole laminates using only the Young's modulus, the strength, and the R-curve of the 0° ply, Composites: Part A 2017; 101: 306–317.

[22] Li, J., Zhang, X. A criterion study for non-singular stress concentrations in brittle or quasi-brittle materials, Engineering Fracture Mechanics 2006; 73: 505–523.

[23] Leguillon, D., Quesada, D., Putot C., Martin, E. Prediction of crack initiation at blunt notches and cavities – size effects. Engineering Fracture Mechanics 2007; 74: 2420–2436.

[24] Hebel, J., Dieringer, R., Becker, W. Modelling brittle crack formation at geometrical and material discontinuities using a finite fracture mechanics approach, Engineering Fracture Mechanics 2010; 77: 3558–3572.

[25] Sapora A., Torabi A.R., Etesam S., Cornetti P. Finite Fracture Mechanics crack initiation from a circular hole, unpublished work submitted to International Journal of Fracture.

[26] Hobbs, D. W. An assessment of a technique for determining the tensile strength of rock. Br. J. Appl. Phys. 1965; 16: 259-268.

[27] Li, D., Wong, L.N.Y. The Brazilian Disc Test for Rock Mechanics Applications: Review and New Insights, Rock Mech Rock Eng 2012; 46: 269–287.

[28] Tada, H., Paris, P., Irwin, G. The stress analysis of cracks. Handbook. second ed., Paris Productions Incorporated, St Louis, MO, USA, 1985.

[29] García, I.G., Mantič, V., Graciani, E. Debonding at the fibre–matrix interface under remote transverse tension. One debond or two symmetric debonds? European Journal of Mechanics - A/Solids 2015; 53: 75-88.

[30] Rosendahl, P.L., Weißgraeber, P., Stein, N., Becker, W. Asymmetric crack onset at open-holes under tensile and in-plane bending loading. International Journal of Solids and Structures 2017; 113–114: 10-23.

[31] Leguillon, D., Yosibash, Z. Failure initiation at V-notch tips in quasi-brittle materials. International Journal of Solids and Structures 2017: 122–123: 1–13.

**Figure caption**

**Figure 1.** BD tests: a) notched sample geometry: the presence of symmetric cracks of length $a$ stemming from the notch tips is also represented; b) stress distribution at the centre of the disk for a plain specimen.

**Figure 2.** BD tested samples: a) $2R$=0.5 mm (PMMA); b) $2R$= 1 mm (PMMA); c) $2R$=2 mm (PMMA); d) $2R$=4 mm (GPPS); e) $2R$= 8 mm (GPPS).

**Figure 3.** Force-extension curves recorded during experiments: a) $2R$=0.5 mm (GPPS); b) $2R$= 2 mm (PMMA); c) $2R$= 8 mm (PMMA).

**Figure 4**. BD notched samples: failure stress according to FFM (continuous line), and to experimental tests on PMMA (plain circles) and GPPS (black circles).

**Figure 5.** Percentage discrepancy between FFM predictions and mean experimental values related to BD tests on PMMA and GPPS notched samples.

**Figure 6**. BD notched samples made of PMMA: FFM critical crack advance obtained by neglecting (thin line) or by considering (thick line) the correction factor (4) for the stress field (3).

**Table caption**

**Table 1.** BD tests: failure loads recorded during experiments on both PMMA and GPPS O-notched samples.